Journal of Applied Research in Water and Wastewater
E-ISSN: 2476-6283
Journal homepage: https://arww.razi.ac.ir

Evaluating the behavior of the Balaroud earth fill dam during impoundment in the final construction stage

Soroush Esmaeili-zadeh, Babak Lashkar-Ara*

Department of Water Engineering, Faculty of Civil Engineering, Jundi-Shapur University of Technology, Dezful, Iran.

GRAPHICAL ABSTRACT

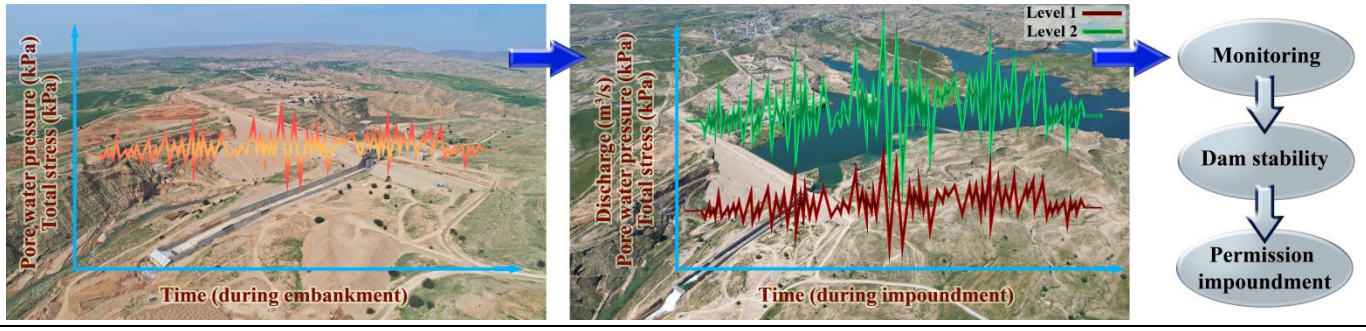

ARTICLE INFO

Article type:
Research Article

Article history:
Received 21 December 2025
Received in revised form 1 March 2025
Accepted 3 March 2025
Available online 1 June 2025

Keywords:
Impounding phase analysis
Instrumented monitoring techniques
Dam stability assessment
Reservoir water level management
Pore water pressure dynamics

Publisher: Razi University

ABSTRACT

Increased demand for freshwater and climate change effects have shifted focus to water resource management, highlighting the crucial role of dams in addressing supply and demand challenges. One of the primary challenges associated with newly constructed dams is effectively monitoring them during the initial phase of impounding. This study investigates the combined performance of the first impoundment period of the Balaroud earth-fill dam concurrently with the final embankment levels of the dam structure. It also explores the simultaneous effects of these factors on the monitoring and stability of the Balaroud dam, providing hydrometric data measurements throughout the process. Analysis of data from the instrumentation located at the critical section of the dam revealed minor variations in the majority of standpipe piezometers and rock piezometers during the initial months of impounding. These variations were exclusively influenced by the embankment of the dam structure. Following the completion of the embankment and the subsequent rise in the reservoir level, the trend of pore water pressure changes has become aligned with fluctuations in the reservoir level. The analysis of data from the embankment piezometer and total pressure cells shows a downward trend in the pore water pressure ratio at the beginning of the impounding phase, which subsequently increased following the completion of the embankment activities and the rise in the reservoir level. During the impounding period, both the maximum pore water pressure ratio and the reliability ratio against liquefaction and internal erosion have remained within permissible and acceptable limits. Additionally, a decreasing trend in the arching ratio was observed in relation to the rising embankment level until its completion. However, as the reservoir level increased and the saturation zone expanded, the arching ratio began to rise again, indicating effective stress transfer within the dam structure despite localized arcing at specific instrumentation points.

1. Introduction

Access to fresh water resources is crucial for human well-being and development. The global population is projected to reach 10.9 billion by 2100, significantly increasing water consumption (Vasconcelos *et al.*, 2015). This rising demand, combined with fresh water scarcity—especially in arid regions—heightens concerns about an impending water crisis. In response, the construction of dams has emerged as a reliable means to secure fresh water supply, serving various purposes such as providing drinking water and generating hydroelectric energy. The total storage capacity of dams worldwide is estimated at approximately 6,000 km^3, highlighting their importance in global water resource management (ICOLD, 2023a).

*Corresponding author Email: Lashkarara@jsu.ac.ir

Research on dams spans multiple disciplines, including hydraulic engineering and environmental science, focusing on their hydraulic behavior, stability, and monitoring during impounding phases. Advanced monitoring and risk assessment methods are essential for ensuring dam safety and optimizing performance. Analyzing displacements, stresses, pore water pressures, and arching ratios is critical for evaluating dam safety and efficiency (Anderson, 1993; Pagano, Desideri and Vinale, 1998). Noteworthy studies on finite element analyses of embankment deformation for zoned earth and rockfill dams have been conducted (Duncan, 1996; Siriwardane and Zaman, 1994). Most analyses are classified as C1 according to Lambe (1973), correlating well with observed behaviors. Additionally, dam safety, particularly regarding overtopping risks during construction, has been extensively studied. Marengo (2006) explored this issue with the

Cite this article: S. Esmaeili-zadeh, B. Lashkar-Ara, Evaluating the behavior of the Balaroud earth fill dam during impoundment in the final construction stage r, *Journal of Applied Research in Water and Wastewater*, 12 (1), 2025, 64-80. doi: https://doi.org/10.22126/arww.2025.11254.1344

Aguamilpa Dam case study, while other studies investigated simulation models and optimization algorithms for reservoir water resource systems, they focused on the optimal exploitation of dams and reservoirs for irrigation and hydroelectric energy purposes (Saab *et al.*, 2022; Chong *et al.*, 2021; Yaseen *et al.*, 2019). The findings underscore the critical role of advanced modeling techniques in enhancing the efficiency and sustainability of water resource management. As water scarcity issues become increasingly pressing, ongoing research aimed at improving dam safety, optimizing water usage, and ensuring environmental sustainability is paramount. Water Resource Management is increasingly recognized as integral to the functionality and sustainability of dam operations. Notably, Nezami and Feizi (2018) emphasized the need for integrated management of groundwater and surface resources, while Salimi *et al.* (2021) demonstrated how scenario analysis can optimize water allocation in the Yamchi Dam basin. Construction practices and stability evaluation are crucial for understanding the long-term performance of earth dams. Cavounidis and Höeg (1977) focused on consolidation behavior during construction, emphasizing the impact of construction techniques on stability. Fetzer, Swiger and Kramer (1988) provided guidelines for earthfill dam construction and foundation treatment. Moreover, Luo *et al.* (2015) investigated the stability effects of the impounding process on the high arch Xiluodu Dam in China. Radzicki and Stoliński (2024) introduced a Multi-Point Thermal-Active Monitoring method for analyzing seepage in earth dams, which overcomes the limitations of traditional linear fiber-optic temperature sensors by utilizing quasi-continuous temperature measurement.

Instrumentation and monitoring are essential for assessing dam stability and performance. Fathi and Golestani (2018) highlighted the correlation between instrumental data and numerical analysis as crucial for accurate monitoring. Eslami, Ghorbani and Shahraini (2020) conducted health monitoring and dynamic analysis at the Siahoo Dam during its initial impounding stage.

Post-construction behavior also contributes significantly to dam safety. Clements (1984) analyzed deformation in rockfill dams, providing insights into deformation mechanisms, while Oral (2010) explored the deformation behavior of a clay-cored rockfill dam in Turkey. Additionally, Yun *et al.* (2022) evaluated dam stability by analyzing pore water pressure and its correlation with reservoir water level fluctuations, revealing a strong linear relationship that aids in assessing dam safety.

In the Sivand dam study, significant conformity was observed between numerical evaluations and observational data, confirming the effective function of the clay core and cutoff wall in response to reservoir level changes. The Eyvashan dam analysis indicated that saturated conditions in the embankment could decrease stability, with elevated pore water pressures at upstream piezometers emphasizing the need for careful management of impoundment rates to maintain dam stability (Komasi and Beiranvand, 2019; Beiranvand and Komasi, 2019). These findings highlight the importance of effective monitoring, robust construction practices, and a proper understanding of post-construction outcomes for the safety and reliability of earth dams.

This study focuses on the monitoring of dam structures and the prediction of their behavior during the impoundment process, particularly concerning the future performance of the dam. Iran's dry and semi-arid climate necessitates the efficient utilization of water resources. The International Commission on Large Dams (ICOLD) reports that Iran ranks 13th globally, with 598 large dams (ICOLD, 2023b) and a cumulative storage capacity of approximately 52,000, 000,000 m^3, with Khuzestan province accounting for 41 percent of this capacity. This underscores the critical role of governmental bodies like the Khuzestan water & power authority in managing these resources.
In this context, several studies have thoroughly investigated sediment management and hydraulic phenomena in the Balaroud river, which is particularly relevant given the region's reliance on water infrastructure. Lashkar-Ara and Kiani (2025) concluded that the Rouse model, which demonstrates an accuracy of 80%, is the most appropriate method for estimating suspended sediment loads in the Balaroud river. Furthermore, Lashkarara, Ghotbi and Armaghani (2012) illustrated that general scour within the river has exposed the foundation of the buried Balaroud inverted siphon structure. The degradation of the riverbed has exacerbated localized scour downstream of the inverted siphon, thereby increasing the likelihood of structural failure. In another study, Fatahi and Lashkar-Ara (2017) demonstrated that soft computing techniques, including artificial neural networks, can be effectively utilized to estimate localized scour downstream of crossing structures within this river.

Among the newly constructed dams is the Balaroud reservoir dam, an earth dam with a vertical clay core located in Iran, in the northern part of Khuzestan Province, near the city of Andimeshk. With 90% of construction completed, the dam faces significant challenges during the initial impounding and testing phases. This context highlights the urgency of the current research project, which aligns with the Khuzestan water & power authority's impoundment schedule that commenced in May 2021.

The innovation of this article lies in its comprehensive examination of the behavior and stability of the Balaroud dam, despite the lack of prior documented monitoring in the scientific literature. The study analyzes the impoundment process in three distinct stages, providing hydrometric data, evaluating pore water pressure monitoring, and analyzing coefficients from theoretical and practical perspectives. Additionally, it thoroughly examines the behavior of arching during embankment construction stages alongside the impoundment process. These analyses will enhance understanding of the dam's dynamic behavior under varying conditions, optimize its management and operational methods, and support the calibration of related numerical models.

2. Materials and methods

2.1. Study area

The Balaroud reservoir dam is situated on the Balaroud river in Iran's Khuzestan province, approximately 27 kilometers north of Andimeshk city. The geographical coordinates of the dam are 48° 16' 18" east longitude and 32° 40' 17" north latitude, with UTM coordinates recorded as 244160 ME and 3618144 MN. This dam is located at the northernmost point of the fertile Khuzestan plain, positioned between the two large dams of Dez and Karkheh. The dam's location is illustrated in Fig. 1. The structure of the Balaroud reservoir dam is classified as an earthen dam featuring a vertical clay core. Currently, it is in the final stages of construction, with 90 percent of the physical work completed. The spillway design of the dam employs an ogee type, equipped with a control gate, which is further enhanced by a chute and a flip bucket, as well as a stepped structure. It is important to note that the gates have not yet been installed; thus, the spillway is currently operated under free control. The characteristics of the Balaroud reservoir dam are summarized in Table 1. In accordance with the criteria established by the ICOLD and the specifications outlined in Table 1, the Balaroud reservoir dam is classified as a large dam (ICOLD, 2023c).

Fig. 1. Location of the Balaroud reservoir dam.

Table 1. Specifications of the Balaroud reservoir dam.

Specifications	Value	Unit
Basin area	696.6	km^2
Dam height from foundation	84	m
Crest length	1054.4	m
Minimum operation level	289	meters above sea level
Spillway ogee level	320	meters above sea level
Reservoir normal level	329.3	meters above sea level
Crest level (embankment final level)	340.5	meters above sea level
Reservoir volume at minimum operation level	8,100,000	m^3
Reservoir volume at spillway ogee level	86,000,000	m^3
Reservoir volume at normal level	131,000,000	m^3
River average yearly discharge	5.4	m^3/s

2.2. Water balance model for reservoir management

According to the plan established by the Khuzestan water and power authority, the impoundment of the Balaroud reservoir dam commenced in May 2021. During this process, due to the incomplete construction of the gates room for the agricultural tunnel, the discharge of the downstream river was managed through the service gate of the bottom outlet tunnel until the reservoir level reached the ogee level of the spillway. In accordance with the limitations outlined in the guidelines for the design and operation of bottom outlets in dam reservoirs, it was stipulated that the service gate should not be operated when the openings are less than 10 percent. Consequently, the impoundment of the Balaroud reservoir dam was planned and executed with three scenarios for the cessation of the impoundment process in mind. The reservoir level was incrementally raised, leading to the establishment of three specific elevation points for the cessation of impounding, defined at 305, 310, and 320 meters above sea level (m.a.s.l). These levels were selected for the purpose of data collection and analysis from the instrumentation installed within the dam's body and foundation. At each defined cessation point in the impounding process, verification and assessment of the data obtained from the instrumentation were conducted to ensure the accuracy of operational conditions and the stability of the dam. This systematic approach also facilitated the necessary conditions for the resumption of the impoundment process and for further raising the reservoir level. It is important to note that the Balaroud river is characterized by two distinct branches located upstream of the dam axis; one of these branches flows into the reservoir from the east, while the other enters from the north. However, no hydrometric stations have yet been established on these rivers, necessitating the use of the water balance method to calculate inlet discharges and validate the methodology.

The water balance model was developed using several essential datasets, which include the level-volume-area curve of the reservoir shown in Fig. 2, the discharge curve of the service gate of the bottom outlet tunnel illustrated in Fig. 3, the discharge curve of the spillway under free flow control represented in Fig. 4, and the evaporation rate of the reservoir depicted in Fig. 5. As detailed in the engineering geology and body analysis reports, the foundation and abutments of the Balaroud reservoir dam have been determined to be impermeable, exhibiting a permeability of less than 3 lugeon. Consequently, the total seepage from the body and foundation of the dam is considered negligible and can be disregarded. For instance, at the normal water level of 329.3 meters above sea level, the seepage rate was calculated to be approximately 0.041 m^3/s. In light of these findings, the water balance model was constructed following the aforementioned processes.

At the start of the impounding process, the reservoir level was recorded by the surveyor using staff gauges installed on the left abutment of the dam. Daily readings were taken by the surveyor during clear weather characterized by sunshine. In cases of precipitation, level readings were conducted at two-hour intervals until the floodwaters receded. Subsequently, the volume of the reservoir was derived from the diagram illustrated in Fig. 2. Furthermore, the discharge released downstream was calculated until the reservoir level rose to the ogee, following the specifications of the bottom outlet tunnel and its opening, as depicted in Fig. 3. If the reservoir level exceeded the ogee, the curve shown in Fig. 4 was used alongside the curve in Fig. 3 to determine discharge rates effectively. Additionally, the volume of water lost to evaporation was quantified and integrated into the overall water balance model, as depicted in Fig. 5. The discharge rate of the river entering the reservoir was determined based on the time interval between two surveyor readings. It was crucial for the quantity of water released from the bottom outlet service gate to satisfy two essential conditions: first, the maintenance of minimal environmental impact downstream, as shown in Fig. 6; and second, compliance with the operational limitations regarding the minimum opening of the service gate of the bottom outlet tunnel. It is important to note that all primary data utilized in this research were calculated and verified by the consulting firm involved in the studies related to both the first and second phases of the Balaroud reservoir dam project.

To validate the accuracy of the water balance model and the calculations of the discharge entering the reservoir, field measurements of the respective discharges from the river inlets were conducted. Given the relatively small cross-sectional areas of the two rivers flowing into the Balaroud dam reservoir and the correspondingly low flow depths, it is reasonable to accept that the flow velocity at a depth of 0.6 m from the free surface can be considered the average velocity for the section. To facilitate this, a cross-section was obtained for each branch of the river using a mapping camera. Subsequently, the velocity of the river flow was measured at this cross-section and at a depth of 0.6 m from the free surface using a velocity meter. Utilizing the measured velocity and the cross-sectional area, the discharge of the river was calculated using Eq. 1.

$$Q = \sum_{n=1}^{i} A_i V_i \quad (1)$$

If the cross-section of the river is divided into `i` sections, where Q represents the total discharge of the cross-section, Ai denotes the area of the i-th section, and Vi signifies the average velocity in the i-th section, then the discharge can be formulated accordingly. For this study, the cross-section was divided into three segments (i = 3), which serves as the basis for calculating discharge as expressed in Eq. 1.

2.3. Instrumentation

To analyze the behavior of the Balaroud reservoir dam during the impounding process, data were collected from nine instrumentation sections installed throughout the dam, with their locations depicted in Fig. 7a. The data used in this research were specifically obtained from the instrumentation of section 4, which represents the maximum embankment section. Fig. 7b illustrates the standpipe piezometers, while Fig. 7c depicts the embankment and rock piezometers along with the total pressure cells installed within this crucial section. This section, corresponding to a range of approximately 642 to 646 m (+0.642 to +0.646 kilometers) from the start of the dam crest, is referred to as section 4.

Given the variety of variables involved in analyzing the instrumentation data, this study focuses on investigating changes in pore water pressure, the pore water pressure ratio, and the arching phenomenon. This focus has enabled a concise analysis that is presented in this paper. The pore water pressure ratio for the piezometers located within the dam body, especially those situated in the clay core, will be calculated using the following equation:

$$PWPR = \frac{u}{\sigma} \quad (2)$$

In this equation, PWPR represents the pore water pressure ratio, u denotes the pore water pressure, and σ signifies the overburden stress. The overburden stress will be derived from the following Eq.

$$\sigma = \gamma . h \quad (3)$$

In this equation, σ represents the overburden stress, γ denotes the unit weight of the embankment materials, and h signifies the height of the embankment measured from the selected reference point. The calculation of Eq. 2, using Eq. 3, is referred to as determining the ratio of measured pore water pressure to theoretical overburden stress (MPWP-T.σ). Conversely, if the overburden stress is measured using

the total pressure cells (TPC) installed within the dam body and incorporated into Eq. 2, it results in the ratio of measured pore water pressure to measured overburden stress (MPWP-M.σ). The arching ratio is defined as the ratio of the measured overburden stress to the computed overburden stress, calculated at any given point based on the height and unit weight of the embankment material. This ratio can be expressed by the following Eq.

$$MTOS = \frac{\sigma}{\gamma . h} \quad (4)$$

In this equation, MTOS denotes the arching ratio: measured to theoretical overburden stress, σ represents the measured overburden stress at the target point, γ indicates the unit weight of the core materials, and h signifies the height of the embankment from the specified point. The data collected from instrumentation across the three impounding scenarios were analyzed. This analysis involved a comparison with values derived from the Balaroud reservoir dam body analysis report, as well as an evaluation against the acceptance criteria established in authoritative references. Such a methodical approach ensured the rigor of the findings, facilitating a detailed understanding of the dam's structural performance. This comparison enabled comprehensive monitoring of the dam during the impounding process.

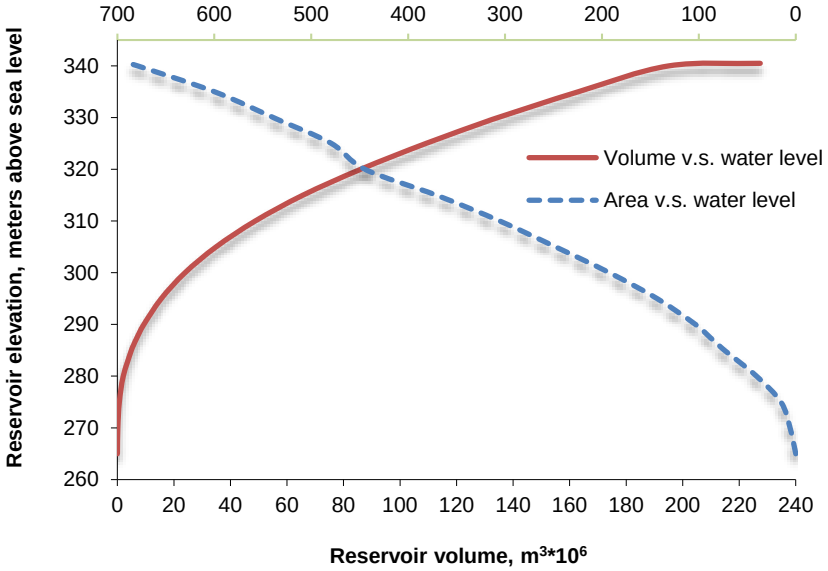

Fig. 2. Volume and area level curves for the Balaroud dam reservoir.

3. Results and discussion

In accordance with the water balance model outlined in the preceding section, the inflows to the Balaroud dam reservoir were systematically measured alongside the initiation of the impounding process. To assess the validity of the aforementioned water balance model, discharge measurements of both inflowing rivers were taken on a clear and sunny day. These empirical data were then compared with discharges calculated by the water balance model. Investigations into the discharge performance revealed a noteworthy discrepancy in the discharge curve of the bottom outlet service gate, particularly observable at low openings (refer to Fig. 3). To rectify this inconsistency, modifications were made to the submergence or orifice coefficient, which significantly improved the alignment between the calculated discharges of the service gate and the actual field measurements. To validate the selection of the submergence or orifice coefficient with precision, field discharge measurements were conducted at a 35 percent opening of the service gate in the bottom outlet tunnel. The collected data were subsequently compared to the adjusted discharge calculations from the water balance model. The results confirmed the accuracy of the selected submergence or orifice coefficient, demonstrating a strong alignment with real observations. The impounding process for the Balaroud reservoir dam commenced in May 2021. By March 2023, the reservoir level had reached the overflow ogee level, situated at an elevation of 320 meters above sea level. Throughout each phase of the impounding process, comprehensive evaluations of all available control systems and instrumentation installed within the dam structure were carried out.

Detailed analyses of the resulting data, along with visual monitoring of both the dam structure and the reservoir, resulted in permission being granted for further elevation of the water level and the continuation of the impounding activities. Ultimately, the absence of the spillway's radial gates led to a significant rise in the reservoir level, reaching approximately 1.75 m above the spillway's ogee level, which is equivalent to 321.75 m above sea level. This situation highlighted the critical importance of ongoing monitoring and adjustment of operational parameters to ensure the stability and safety of the dam structure throughout the impounding process.

3.1. Hydrometric and hydrological trends during the impounding of the reservoir

As previously noted, the impounding process for the Balaroud reservoir dam began in May 2021, marking the first water year for impounding. However, contrary to expectations, the reservoir level did not consistently rise until December 2021 in the second water year and November 2022 in the third water year. This sequence of events resulted in an extended impounding period that spanned three consecutive water years. In the first water year, the impounding was halted during the first scenario at Level 305 due to insufficient precipitation and drought conditions. Consequently, the reduced river discharge, combined with the restrictions on the opening of the service gate in the bottom outlet tunnel, caused a rapid decline in the reservoir level, ultimately leading to its complete depletion.

This state persisted until the onset of the third water year. However, in November 2022, a significant increase in precipitation was observed in the basin area. By February 13, 2023, the impounding process reached the second stop scenario, and on March 29, 2023, the third stop scenario was achieved. Consequently, the reservoir level was raised to 321.75 meters above sea level on April 13, 2023, marking the highest recorded water level in the Balaroud dam reservoir to date. Given the substantial portion of the impounding process that occurred during the third water year, a thorough evaluation and analysis of the hydrometric and hydrological data from this year have been conducted.

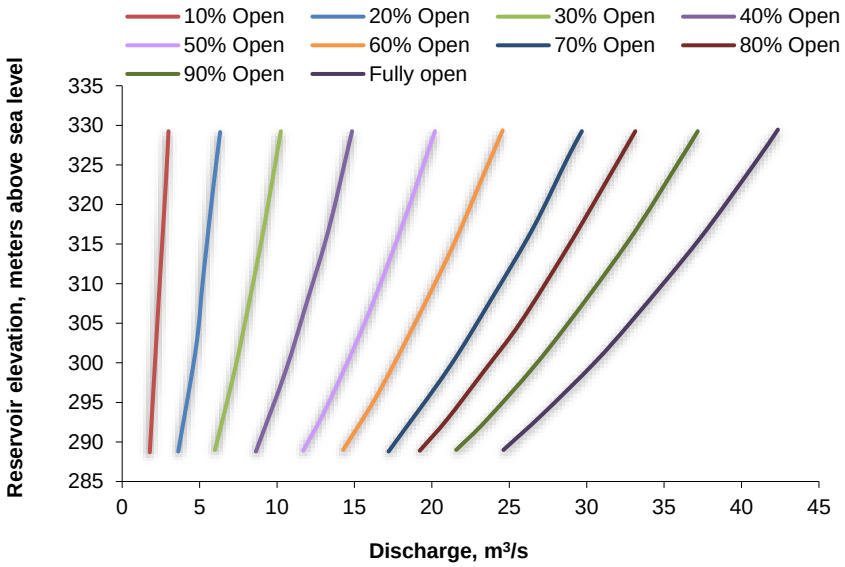

Fig. 3. Discharge curves for the bottom outlet tunnel service gate at various opening percentages.

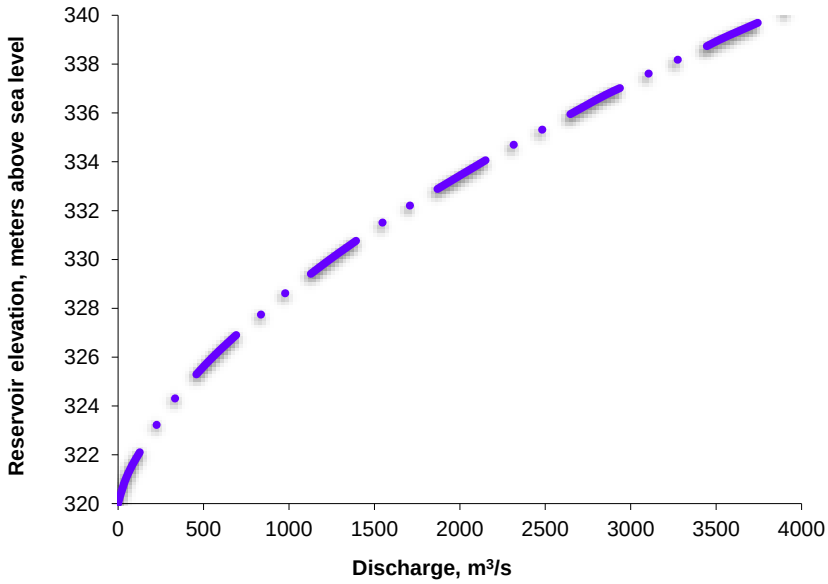

Fig. 4. Spillway discharge curve under free flow conditions.

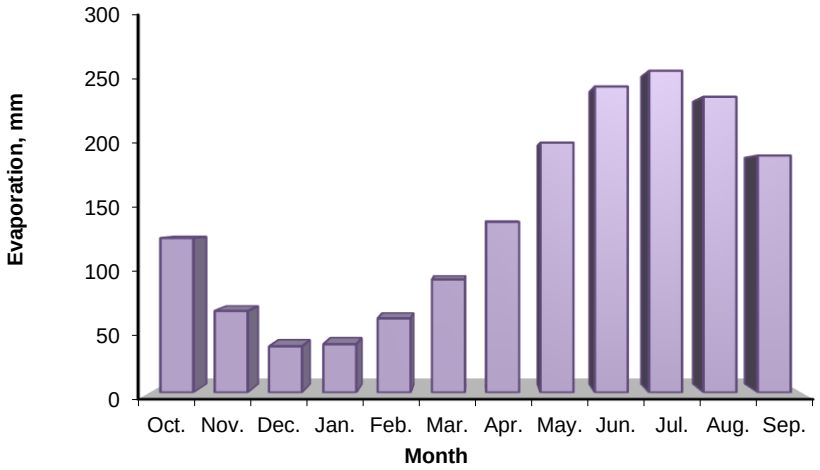

Fig. 5. Monthly evaporation from the surface of the Balaroud dam reservoir.

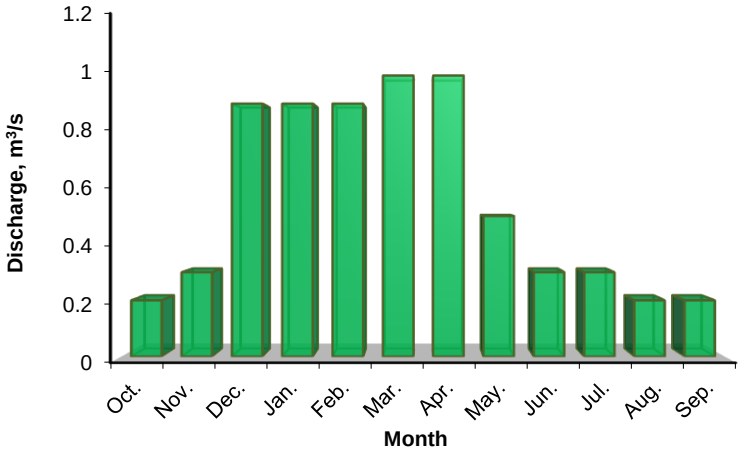

Fig. 6. Minimum discharge levels essential for maintaining downstream environmental conditions.

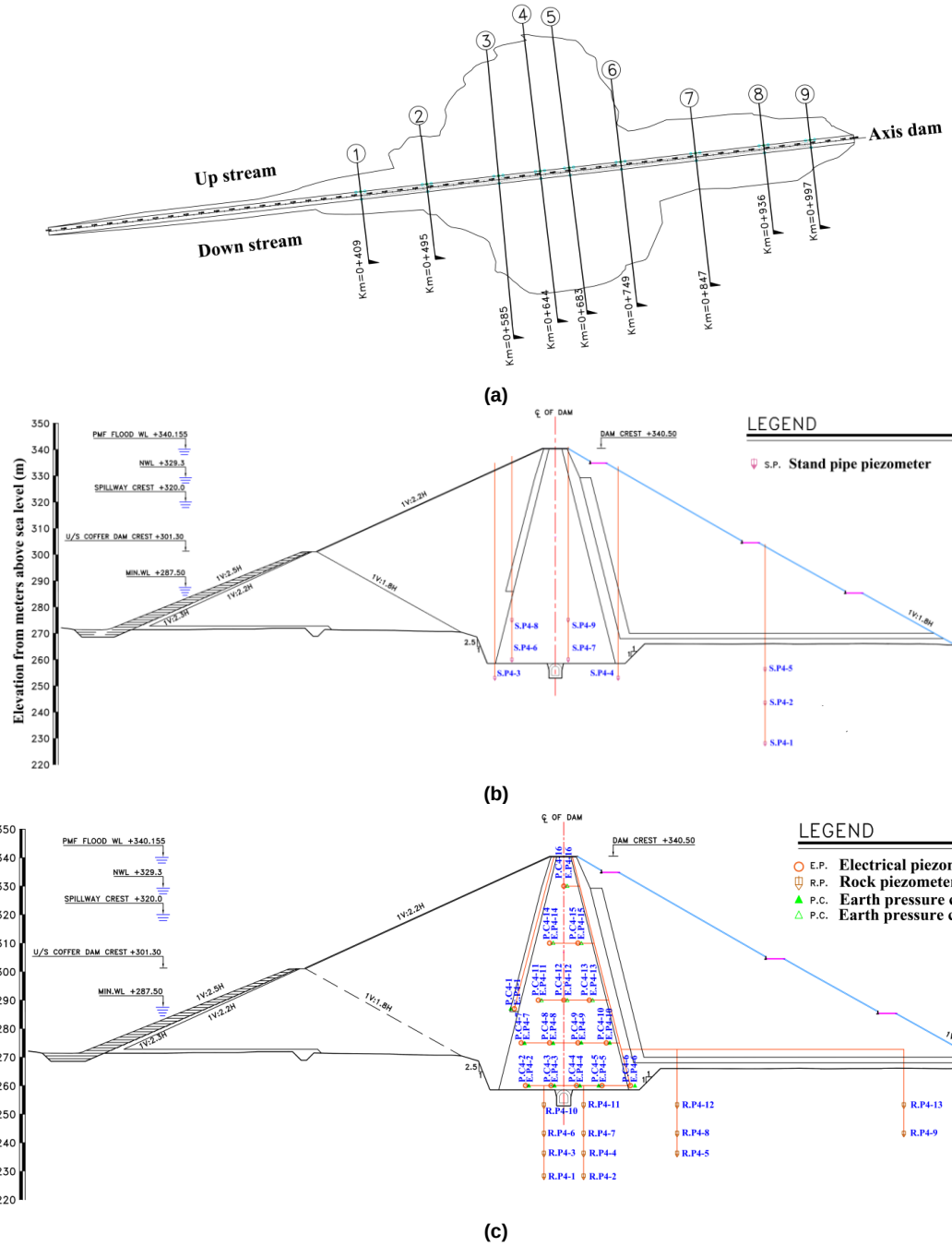

Fig. 7. Locations of instrumentation at Balaroud dam: (a) Nine instrumentation sections, (b) Standpipe piezometers in section 4, (c) Embankment, rock piezometers and total pressure cells, in section 4.

Figs. 8 and 9 provide a detailed depiction of the volume of water inflow and outflow from the reservoir during the third water year, organized by month. As illustrated in Fig. 8, the total volume of inflow into the reservoir throughout the impounding process was recorded at 213,000,000 m^3, representing a notable increase of 63 percent compared to the normal reservoir volume of 131,000,000 m^3, and a 25 percent increase relative to the yearly river discharge volume at the dam axis of 170,000,000 m^3. Furthermore, it is indicated that 35 percent of the total inflow volume entered the dam reservoir specifically during April 2023, a month in which the inflow from the Balaroud river at the dam axis constituted 56.5 percent of the normal reservoir volume. This observation suggests the occurrence of exceptionally favorable hydrological conditions within the basin area. Fig. 9 illustrates the total outflow volume from the reservoir during the third water year. The data presented in this chart indicates that the total outflow volume was 127,000,000 m^3, with 41 percent of this outflow occurring in April 2023.

Fig. 10 illustrates the average monthly discharge for both the inflow and outflow of the Balaroud reservoir, comparing these metrics against the normal river discharge for each month of the third water year. An analysis of the data indicates that, with the exception of December and March, the average monthly inflow discharge to the reservoir consistently surpassed the normal discharge of the river. Notably, in April 2023, the river recorded its maximum discharge, reflecting a dramatic increase of 201.5 percent compared to the normal discharge. Historically, the average yearly discharge at the dam axis has been documented at 5.4 m^3/s. However, during the third water year, this figure surged by 126 percent, reaching an enhanced average of 6.8 m^3/s. Regarding outflows, the average monthly discharge from the reservoir remained below the normal river discharge from October 2022 through March 2023. This decrease is attributed to the operational constraints of the service gate, which maintained a minimum environmental discharge. Conversely, from April 2023 onward, the outflow discharge exceeded the normal river discharge. A closer examination of Fig. 10 underscores the significant impact of the Balaroud reservoir's impounding on downstream river discharge, particularly during the warm and dry seasons. In the months of April, May, June, July, August, and September, the downstream river discharge increased markedly: 140 percent, 159 percent, 139 percent, 148 percent, 148 percent, and 165 percent, respectively, compared to normal discharges for those months. This sustained increase in downstream discharge coincides with the final months of the precipitation season in the basin, which is critical for agricultural irrigation. The increased river discharge during this period highlights the reservoir's essential role in meeting irrigation demands, particularly since the irrigation and drainage network was not yet fully operational at that time. The implications of this hydrological change are complex, as the enhanced water availability not only supports agricultural activities but also has significant effects on the downstream river ecosystem. The steady discharges managed by the reservoir can help maintain ecological health during drier periods, ensuring that aquatic habitats are preserved and supported throughout the dry season cycle. Overall, the Balaroud reservoir's impounding is crucial for managing water resources for agricultural and ecological sustainability in the region.

Fig. 11 illustrates the hydrographs of the inlet floods into the Balaroud reservoir during the third water year. Notably, the outflow hydrographs were not generated simultaneously with the inflow hydrographs until the end of March 2023. This delay was mainly due to the intentional control of the minimum outflow discharge from the dam during this period. As the reservoir level reached the ogee level of the overflow in April 2023, spillway activation permitted an increase in outflow discharge from the dam. Consequently, Fig. 11 exclusively features the outflow hydrograph for April 2023. The data presented indicates that the maximum peak of the inflow flood during the impounding process occurred in April, measuring 677 m^3/s. This peak discharge corresponds to a flood event with a return period of approximately two years. In addition to the significant peak in April, inlet floods were also recorded in the preceding months of February, January, and March 2023, with peak discharges of 405, 248, and 176 m^3/s, respectively. The hydrograph for the outflow discharge from the dam in April 2023 reveals a notable reduction of 81 percent from the peak inflow flood. This substantial decrease emphasizes the reservoir's ability to mitigate flood intensity, highlighting its critical role in flood management. Moreover, this observation underscores the temporal offset between the peak inflow flood and the peak outflow discharge, which is an essential feature of the reservoir's flood control functionality. During the active outflow discharge in April 2023, both the ogee spillway and the bottom outlet tunnel contributed to the outflow discharge. It is important to note that over 30,000,000 m^3 of water were released downstream exclusively through the ogee spillway, reflecting the infrastructure's capacity to effectively manage and release water volumes during flood events. Overall, the data presented in Fig. 11 underscores the reservoir's pivotal role in regulating inflow and outflow, protecting downstream areas from potential flooding while also facilitating irrigation and ecological maintenance during critical periods. Such capabilities significantly enhance the reservoir's effectiveness as a vital water management resource in the region.

3.2. Investigation of changes in pore water pressure

The instrumentation of the Balaroud reservoir dam includes electric vibrating wire piezometers (RP & EP) and casagrande standpipe piezometers (SP) to accurately measure pore water pressure within both the dam body and its foundation. These instruments are commonly utilized for evaluating piezometric pressure, with vibrating wire piezometers being particularly effective at measuring pore water pressure in challenging conditions. Conversely, casagrande standpipe piezometers provide a simple and cost-effective approach for monitoring pore water pressures and water levels.

Data collection from these instruments began at the start of the impounding process, coinciding with the final embankment of the dam structure. For the vibrating wire piezometers, measurements were taken daily as the reservoir level was gradually raised. Once the reservoir level stabilized and the dam body was actively being embanked, the measurement frequency was adjusted to twice a week.

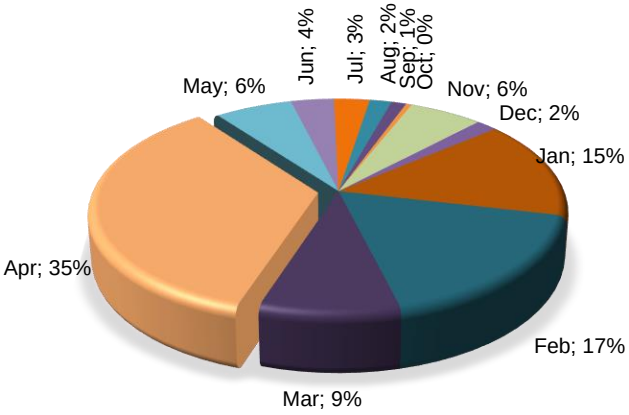

Fig. 8. Total inflow volume to Balaroud dam reservoir during the third water year (September 23, 2022 - September 22, 2023): 213,000,000. m^3.

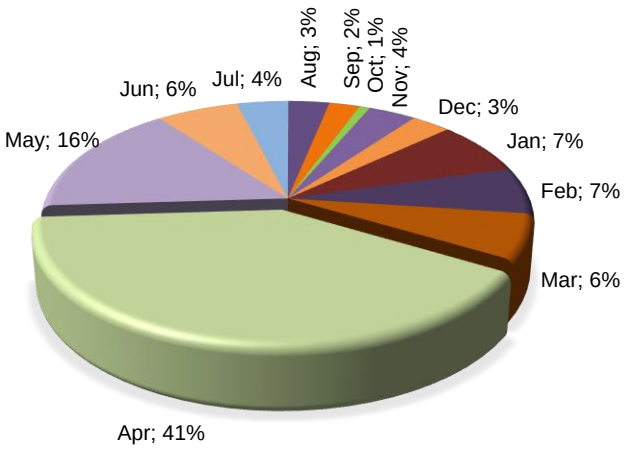

Fig. 9. Volume of water released from Balaroud dam reservoir during the third water year (September 23, 2022 - September 22, 2023): 127,000,000 m^3.

Similarly, the casagrande standpipe piezometers adhered to a measurement schedule of twice a week during periods of rising or stabilizing reservoir levels. When the dam body was being embanked while the reservoir remained empty, measurements from the casagrande piezometers were conducted once a week.

The pore water pressure within the dam's core is primarily influenced by two key factors: 1) loading: This includes the increase in stress resulting from the final embankment of the dam body during construction, as well as dynamic loads that may arise from seismic activity. 2) changes in reservoir water level: Fluctuations in the water level of the reservoir significantly affect pore water pressure dynamics. According to the findings outlined in the second phase of studies titled "dam body analysis report," the maximum pore water pressure calculated at the completion of the Balaroud reservoir dam's construction reached 800 kilopascals. This peak pressure occurs within the clay core of the dam, specifically at a depth of 74.17 m from the dam's crest. This investigation into pore water pressure changes is essential for understanding the stability and performance of the dam structure under various loading conditions and during operational phases. Continuous monitoring through the employed instrumentation will enable timely assessments and necessary interventions to ensure the dam's integrity and safety throughout its operational lifespan.

3.2.1. First stage impoundment

The first stage of impoundment takes place at an elevation of 305 meters above sea level (m.a.s.l). Changes in the pore water pressure curve during this process are illustrated in Fig. 12a, particularly focusing on the piezometers installed at an elevation of 227 m.a.s.l., which were assessed as key indicators. The elevation of 227 meters above sea level represents the lowest installation level of the precision instruments, and due to its placement in the dam foundation, it is crucial for dam behavior monitoring studies. The data presented includes readings from instrumentation located in section No. 4, which has the maximum embankment, and from section No. 5, located between 683 m and 687 m from the beginning of the dam crest, which also features significant embankment heights. Analysis of the figure reveals that from May to December 2021, there was a gradual increase in pore water pressure across all vibrating wire piezometers and casagrande standpipe piezometers, with the exception of the SP 5-1 piezometer. This slow increase in pore water pressure can be attributed to the ongoing embankment of the dam body during this period, resulting in a corresponding rise in the embankment curve. The construction activities created additional stress, leading to a gradual accumulation of pore water pressure. After December 2021, as the reservoir level continued to rise, a more pronounced increase in pore water pressure was observed across all piezometers. This trend validated the proper functioning of the installed instrumentation. Notably, the highest measured pore water pressure was for the vibrating wire piezometer RP 5-2, located downstream, which registered a value of 792.32 kilopascals. This measured pressure, while significant, remains below the maximum pore water pressure noted in the dam body analysis report.

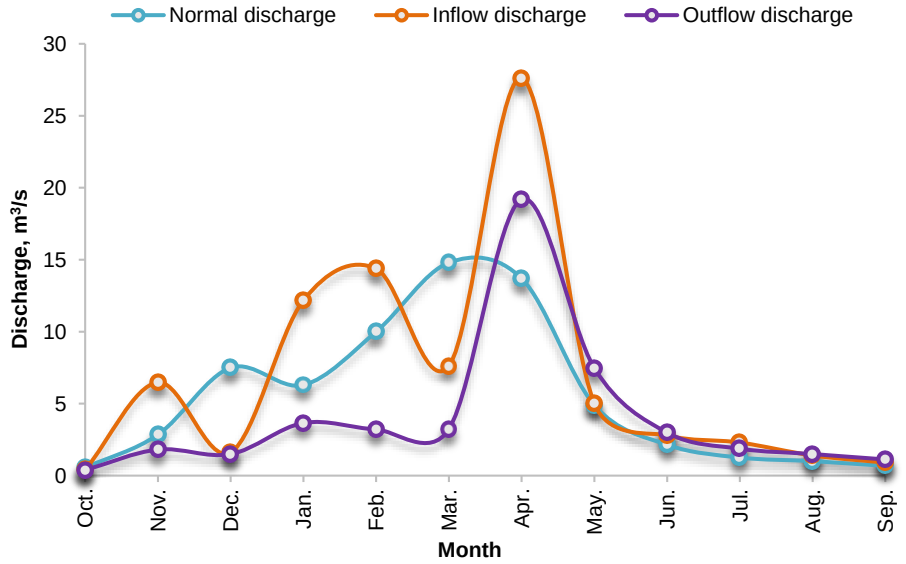

Fig. 10. Average monthly discharge curve of the Balaroud river during the third water year (September 23, 2022 - September 22, 2023) compared to normal discharge.

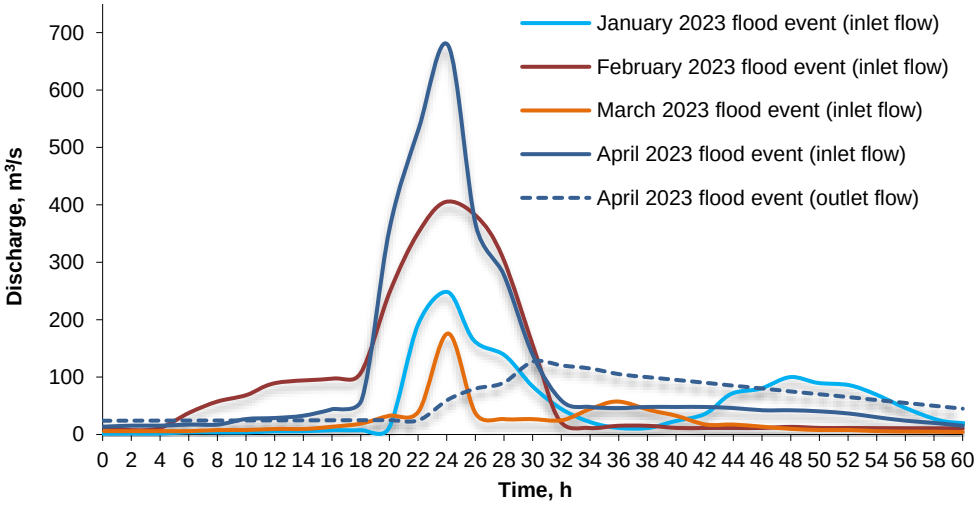

Fig. 11. Hydrographs of specific flood events during the impounding process.

3.2.2. Second stage impoundment

The second stage of impoundment occurs at an elevation of 310 meters above sea level (m.a.s.l). Changes in the pore water pressure curve during this process are depicted in Fig. 12b, particularly highlighting the piezometers installed at an elevation of 227 m.a.s.l., which were identified as key indicators. As the impoundment process advanced and the dam body embankment was completed, the variations in piezometer readings were primarily attributed to changes in the reservoir level. In March 2022, a decline in the reservoir level was noted, which was accompanied by a corresponding decrease in pore water pressure. This trend persisted until November 2022, when the

onset of precipitation led to a rise in the reservoir water level, subsequently resulting in an increase in pore water pressure. In March 2023, the highest pore water pressure measured was at the RP 5-2 vibrating wire piezometer, located downstream. This measurement reached 842.70 kilopascals, indicating a significant increase compared to previous measurements. Notably, the pore water pressure measured was 5.34 percent higher than the maximum pore water pressure reported in the dam body analysis report. Despite this increase surpassing the maximum value, no abnormal conditions were observed, as this rise in pore water pressure did not coincide with an increase in overburden stress within the total pressure cell (TPC) situated at the same location.

3.2.3. Third stage impoundment

The third stage of impoundment occurs at an elevation of 320 meters above sea level (m.a.s.l). Changes in the pore water pressure curve during this process are illustrated in Fig. 12c, particularly emphasizing the piezometers installed at an elevation of 227 m.a.s.l., which were identified as key indicators. As the impounding process advanced, the variation pattern of the piezometers was found to be closely associated with changes in the reservoir level. This relationship became especially evident during the third stage of impounding, observed in March 2023. An increase in the reservoir level during this period led to a corresponding rise in pore water pressure, a trend that continued until April 2023. In April 2023, the highest pore water pressure measured was at the RP 5-2 vibrating wire piezometer located downstream. This measurement reached 888.74 kilopascals, marking a significant increase in pressure compared to previous measurements. Notably, the measured pore water pressure was found to be 11.10 percent higher than the maximum pore water pressure documented in the dam body analysis report. Despite this elevated pressure exceeding the maximum threshold, no abnormal conditions were reported. It was noted that this increase in pore water pressure did not coincide with a rise in overburden stress within the total pressure cell (TPC) at the same location.

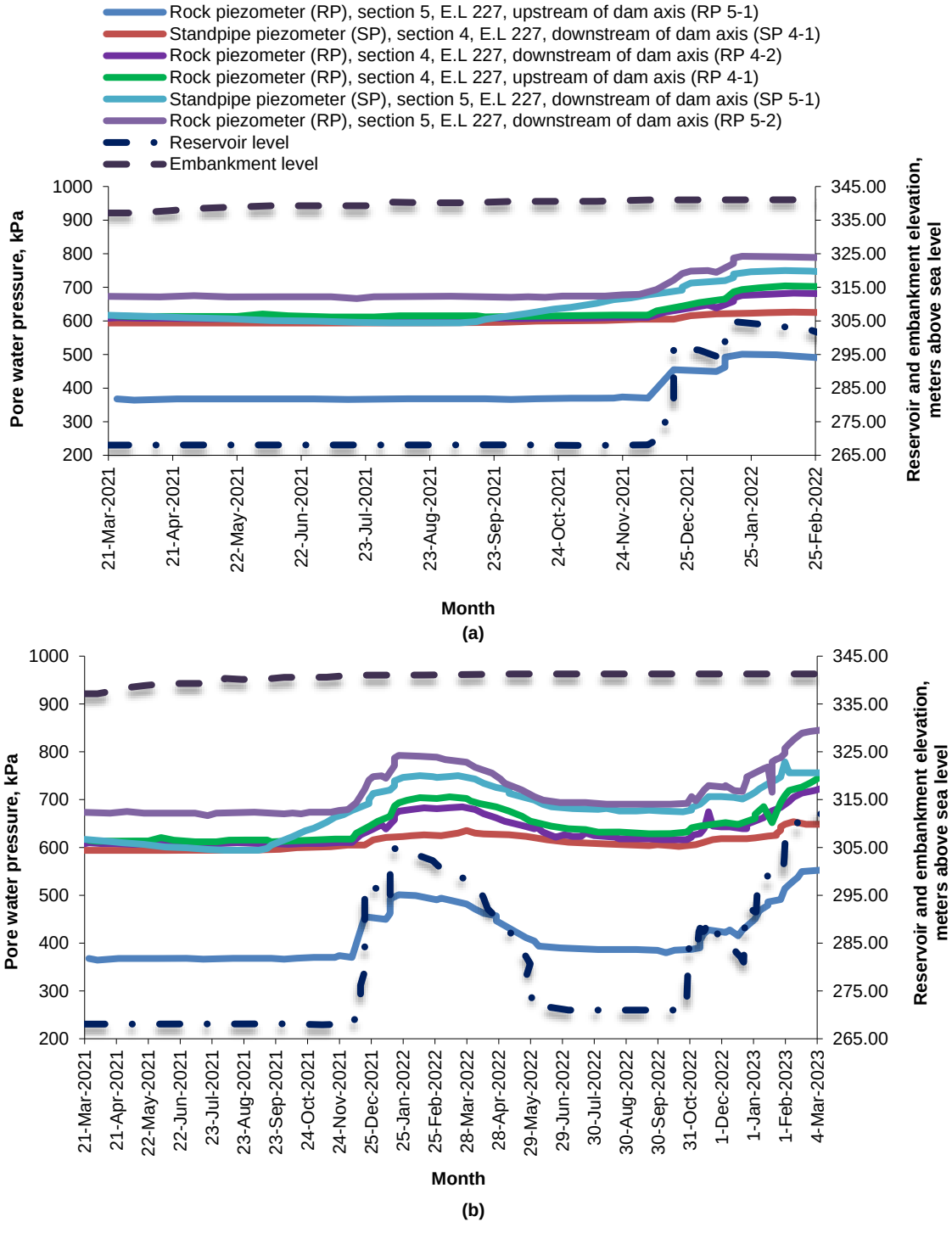

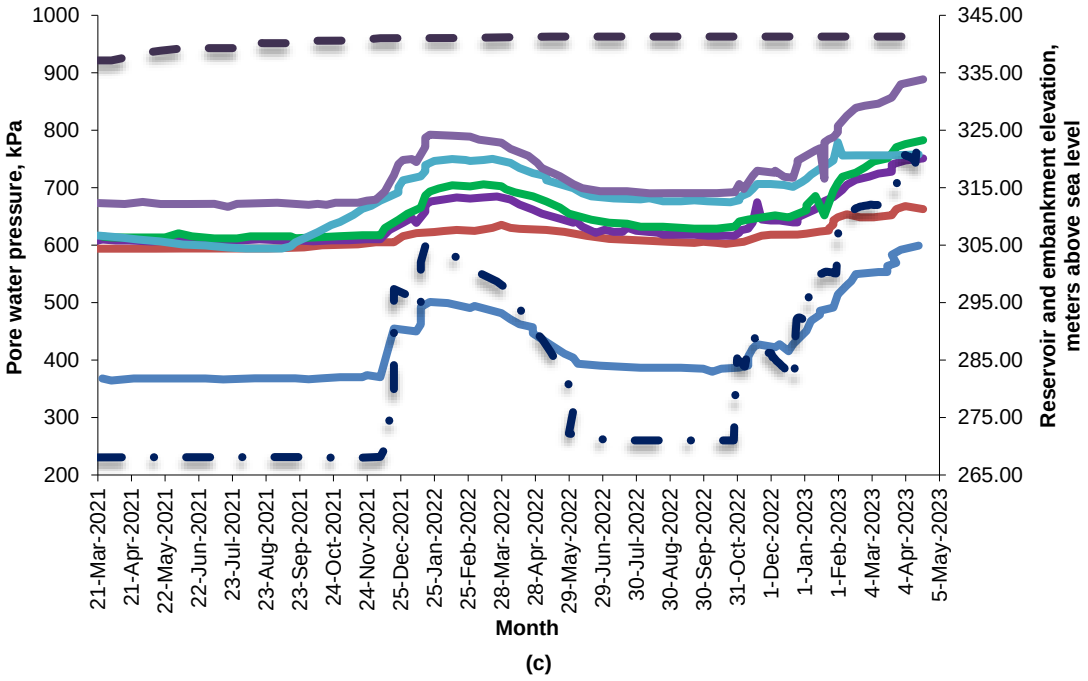

Fig. 12. Changes in pore water pressure during the (a) first, (b) second, and (c) third stages of impoundment.

3.3. Investigation of changes in pore water pressure ratio (PWPR)

In the instrumentation design of the Balaroud reservoir dam, total pressure cells (TPC) equipped with stress gauge pressure transducers have been utilized to determine the overburden stress. The overburden stress was calculated by transferring the measured pressure from the pressure pad (total pressure cells) to a stainless steel tube connected to a stress gauge pressure transducer. Subsequently, the pore water pressure, measured at the same location using vibrating wire piezometers, was subtracted from the overburden stress (in the vertical direction), yielding the effective stress. At the onset of the impounding process, and concurrently with the embankment of the final levels of the dam body, data collection for the vibrating wire piezometers was conducted daily, corresponding with the rise in reservoir water levels. In cases where the reservoir level stabilized while the dam body embankment was actively ongoing, the frequency of data collection was adjusted to twice weekly. Likewise, data collection from the total pressure cells (TPC) was performed biweekly, aligned with the periods of reservoir level increase or stabilization and the ongoing embankment of the dam body. One of the most critical aspects of monitoring and controlling the stability of earth-fill and rock-fill dams with a clay core is the necessity to evaluate the development of pore water pressure within the dam core. An excessive increase in pore water pressure can lead to a reduction in effective stress, which subsequently diminishes the stability of the dam and heightens the potential for long-term settlements within the dam core. Based on the maximum pore water pressure within the core and the depth at which it occurs, as previously referenced in the report "Balaroud reservoir dam - dam body analysis report," the ratio of measured pore water pressure to theoretical overburden stress (MPWP-T.σ) at the conclusion of dam construction was calculated to be 0.521, in accordance with Eq. 2. The acceptance criterion for the pore water pressure ratio (PWPR) stipulates that it should remain below 0.5 under normal conditions and below 0.7 under extreme loads (Fell *et al.*, 2015). Furthermore, according to Sharma (1991) diagram, the permissible range for the PWPR of a clay core with an optimal moisture content of 18 percent lies between 0.4 and 0.6 (Sharma, 1991). The core of the Balaroud reservoir dam was also constructed under similar optimal moisture content conditions, making the value of 0.521 fully acceptable. It is important to note that when the PWPR approaches 1, it indicates that the pore water pressure is equivalent to the overburden stress, significantly increasing the likelihood of hydraulic fracturing occurring within the dam structure. Therefore, continuous monitoring of the PWPR remains essential to ensure the long-term stability and safety of the Balaroud reservoir dam.

3.3.1. First stage impoundment

The first stage of impoundment occurs at an elevation of 305 meters above sea level (m.a.s.l). Changes in MPWP-T.σ and the ratio of measured pore water pressure to measured overburden stress (MPWP-M.σ) during this process are depicted in Fig. 13a and Fig. 14a. The data presented in these figures were analyzed based on measurements obtained from section No. 4. From May to December 2021, when the reservoir was empty, as shown in Fig. 13a, the MPWP-T.σ exhibited a notable decline at all measurement locations, characterized by a minimal rate of change. The observed stability in pore water pressure, coupled with the increase in height due to the embankment of the dam body final levels represented by increasing h, indicates a slight decrease in MPWP-T.σ during this construction period. Between December 2021 and March 2022, the onset of precipitation and the subsequent rise in reservoir levels led to an increase in MPWP-T.σ due to elevated pore water pressure (u) at select piezometers located in the upstream portion of the dam, which include EP 4-1, EP 4-2, and EP 4-7. In contrast, MPWP-T.σ remained relatively constant in the remaining piezometers. This discrepancy is attributed to the proximity of the upstream piezometers to the reservoir; hence, they respond to changes in pore water pressure earlier than the downstream piezometers, as reflected in their MPWP-T.σ values. The maximum MPWP-T.σ value was calculated at the EP 4-9 piezometer, at 0.29, which is below the specified acceptance criterion for PWPR, which is 0.521, at the time of dam construction completion. Similarly, from May to December 2021, the MPWP-M.σ, as illustrated in Fig. 14a, also demonstrated a significant decline across all locations, with a minimal rate of change. The measured increase in overburden stress in TPC cells, resulting from the dam body embankment during construction, is illustrated in the embankment curve of Fig. 14a. This, along with the stability of pore water pressure, contributed to a slight decrease in MPWP-M.σ. From December 2021 to March 2022, as precipitation began and reservoir levels rose, MPWP-M.σ values increased in several piezometers located in the upstream section of the dam, including EP 4-1, TPC 4-1, EP 4-2, TPC 4-2, and EP 4-7, TPC 4-7, due to the rise in pore water pressure (u). Meanwhile, MPWP-M.σ remained relatively constant at other dam body locations, excluding EP 4-14, TPC 4-14, and EP 4-16, TPC 4-16. The stability in these values can again be linked to the geographical position of the mentioned piezometers, which, being above the impounding level of 305 meters above sea level, experienced reduced influence from pore water pressure, resulting in negligible changes in MPWP-M.σ. The maximum ratio obtained for MPWP-M.σ was at the EP 4-4, TPC 4-4 point, with a value of 0.50, which also falls below the acceptance criterion of PWPR, set at 0.521. A comparative analysis of Fig. 13a and Fig. 14a indicates that the rates of change for MPWP-T.σ and MPWP-M.σ are aligned; however, MPWP-T.σ values consistently remain lower than MPWP-M.σ values at all measurement points throughout the discussed time frame. This discrepancy is likely due to a local arching phenomenon observed at the installation site of the TPC cells, which has resulted in lower measured overburden stress than expected. The average difference between MPWP-M.σ and MPWP-T.σ values is 0.16, suggesting that constrained excavation conditions during TPC installation, along with insufficient space for proper embankment compaction, may have

contributed to this phenomenon. While a definitive assessment of the local arching phenomenon cannot be made at this stage of the impounding process, it is expected that over time, as the impounding process continues and the dam body settles within permissible limits, the local arching effect will dissipate, bringing the measured overburden stress value closer to its true value.

3.3.2. Second stage impoundment

The second stage of impoundment occurs at an elevation of 310 meters above sea level (m.a.s.l). Changes in MPWP-T.σ and MPWP-M.σ during this process are illustrated in Fig. 13b and Fig. 14b, based on data obtained from section No. 4. As the impounding process progressed and the dam body embankment neared completion, the changes in the piezometers beginning in March 2022 were primarily influenced by the reservoir level, as shown in Fig. 13b. The stabilization and reduction of the reservoir level led to a decrease in MPWP-T.σ, which remained constant in some piezometers until November 2022. The onset of precipitation and the subsequent rise in the reservoir level from November 2022 triggered a gradual increase in MPWP-T.σ that continued until March 2023. From March 2023 onward, with ongoing precipitation and rising reservoir levels, MPWP-T.σ values in several upstream piezometers, including EP 4-1, EP 4-2, EP 4-7, EP 4-11, and EP 4-12, began to rise due to increased pore water pressure u. In contrast, MPWP-T.σ remained stable in the other piezometers. This effect is attributed to the upstream piezometers' proximity to the reservoir, allowing them to respond to changes in pore water pressure more quickly than their downstream counterparts. The maximum MPWP-T.σ value calculated was at the EP 4-9 piezometer, with a value of 0.28, which is still below the specified acceptance criterion for PWPR at the completion of dam construction of 0.521. Fig. 14b illustrates that the decline and stabilization of the reservoir level between March 2022 and November 2022 coincided with a decrease in MPWP-M.σ across all points of the dam body, at times reflecting a state of relative constancy. Given the completion of the dam body's embankment during this period and the lack of significant changes in overburden stress measured by the TPC cells, it can be concluded that the observed MPWP-M.σ levels are primarily influenced by variations in pore water pressure. Thus, as pore water pressure decreased, MPWP-M.σ values also diminished. From November 2022 to March 2023, the onset of precipitation and an increase in the reservoir level resulted in rising MPWP-M.σ values at most upstream piezometers, attributed to increased pore water pressure. The maximum obtained MPWP-M.σ value was at the EP 4-3, TPC 4-3 point, at 0.517, which remains below the acceptance criterion for PWPR at 0.521. A comparative analysis of Fig. 13b and Fig. 14b reveals that the rates of change for MPWP-T.σ and MPWP-M.σ are closely aligned. However, MPWP-T.σ values consistently remain lower than MPWP-M.σ values across all measurement points and the entire observed period. This discrepancy can be attributed to the local arching phenomenon at the TPC cell installation site, which results in the recorded overburden stress being lower than expected.

The average discrepancy between the MPWP-M.σ and MPWP-T.σ values stands at 0.14, which is slightly less pronounced than the 0.16 discrepancy observed during the first phase of impounding. It is anticipated that over time, as the impounding process progresses and the dam body settles within permissible limits, the local arching phenomenon will dissipate, leading to measured overburden stress values that are closer to the actual values.

3.3.3. Third stage impoundment

The third stage of impoundment occurs at an elevation of 320 meters above sea level (m.a.s.l). Changes in MPWP-T.σ and MPWP-M.σ during this process are illustrated in Fig. 13c and Fig. 14c. The analysis presented in these figures is based on data obtained from section No. 4. During March 2023, the observed changes in the piezometers were entirely dependent on the reservoir level, as shown in Fig. 13c. Consequently, as the reservoir level increased, MPWP-T.σ values also rose, maintaining this trend until April 2023. Notably, the most significant changes in MPWP-T.σ values were calculated in the piezometers EP 4-1, EP 4-2, EP 4-7, and EP 4-11. The proximity of these upstream piezometers to the reservoir enables them to respond more promptly to changes in pore water pressure, thereby assuming their role earlier than the downstream piezometers. The highest calculated MPWP-T.σ value, attributed to the EP 4-1 piezometer, was 0.32, which remains below the specified acceptance criterion for PWPR at dam construction completion, set at 0.521. As illustrated in Fig. 14c, MPWP-M.σ increased across the majority of points within the dam body throughout March 2023. Given the completion of the dam body embankment during this timeframe and the absence of significant changes in overburden stress from TPC cells, it can be inferred that MPWP-M.σ values are substantially influenced by pore water pressure. Thus, as pore water pressure rises, MPWP-M.σ also increases. The maximum obtained MPWP-M.σ value was at the EP 4-2, TPC 4-2 point, at 0.475, which also remains below the acceptance criterion for PWPR at 0.521. A comparative analysis of Fig. 13c and Fig. 14c indicates that the rates of change in MPWP-T.σ and MPWP-M.σ are consistent. However, MPWP-T.σ values are consistently lower than MPWP-M.σ values across all measurement points and throughout the entire observation period. This discrepancy is attributed to the local arching phenomenon occurring at the TPC cell installation points, which results in measured overburden stress being lower than the expected values.

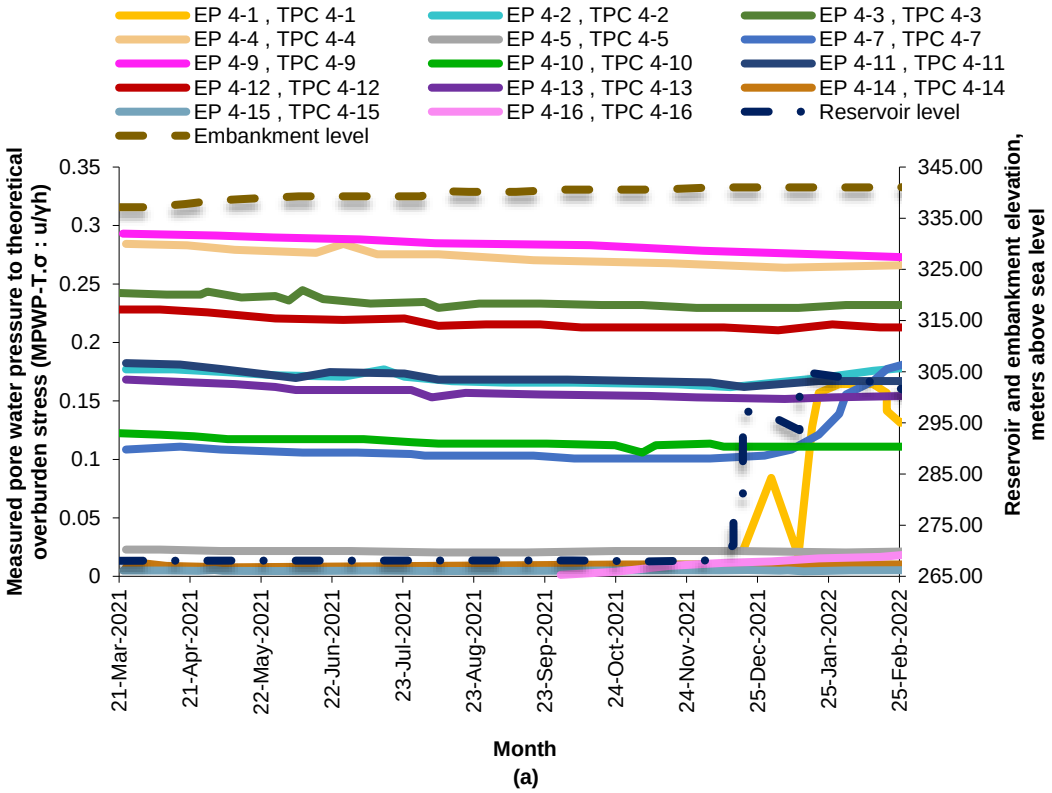

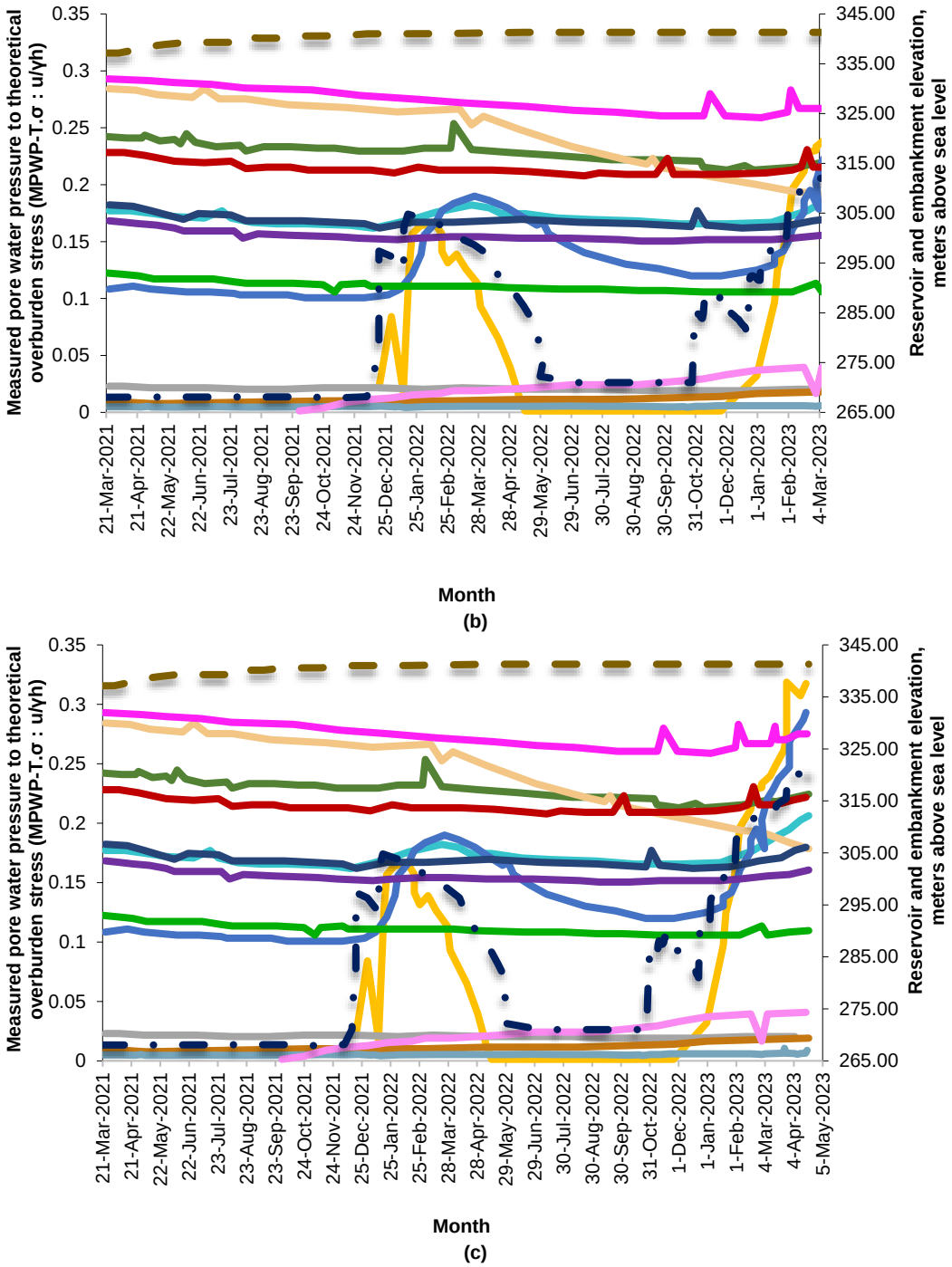

Fig. 13. Changes in the ratio of measured pore water pressure to theoretical overburden stress (mpwp-t.σ) during the (a) first, (b) second, and (c) third stages of impoundment.

Note: E.P. stands for "embankment piezometer" and T.P.C. stands for "total pressure cell." The numbers indicate their installation positions in the dam structure (refer to Fig. 7c).

The average discrepancy between MPWP-M.σ and MPWP-T.σ values is 0.10, which is less pronounced compared to the discrepancies observed during the first and second stages of impounding, which were 0.16 and 0.14, respectively. It is anticipated that, over time and with continued impounding to a normal level of 329.3 meters above sea level, along with the settlement of the dam body within permitted limits, the effects of local arching will diminish, allowing measured overburden stress to approach their true values. It was noted that the ratios of MPWP-M.σ and MPWP-T.σ at all points of the dam body remained below the maximum allowable PWPR of 0.521. To accurately assess the impact of the PWPR on dam stability, particularly concerning the safety factor related to the potential for liquefaction and internal erosion, the ratio of overburden stress to pore water pressure (1/PWPR) is essential. According to available references, the ratio of 1/PWPR should be greater than 1.5 (Fell *et al.*, 2015; USBR, 2014). The findings indicate that the highest PWPR occurred at the MPWP-M.σ point EP 4-3, PC 4-3 during the second impounding stage, with a value of 0.517. Consequently, the maximum computed ratio of 1/PWPR is determined to be 1.93, which surpasses the minimum threshold of 1.5. In light of these observations, the likelihood of liquefaction and internal erosion occurring within the Balaroud reservoir dam is considered low.

3.4. Investigation of changes in arching phenomenon

The arching action is a critical phenomenon that occurs during both the construction and operational phases of dams. In earthfill dams, especially those with a clay core, the differential stiffness between the clay core and the surrounding filter media can result in uneven settlement. This differential settlement significantly influences the transfer of stress within the dam body. A lower arching ratio: measured to theoretical overburden stress (MTOS) indicates inadequate stress transfer from the embankment to the underlying layers, while a higher ratio signifies effective stress transfer from the upper layers to the lower layers. When analyzing the geometric configurations of the dam, it can be observed that if the width of the valley beneath the dam is less than 0.25 times the dam's height, and the slope of the valley exceeds 60 degrees, there is a substantial probability of both vertical and horizontal arching. Conversely, in situations where the valley width exceeds 0.75

times the dam height and the valley slope is greater than 45 degrees, the likelihood of horizontal arching becomes sufficiently minimal to be considered negligible (Fell *et al.*, 2015). Given that the Balaroud reservoir dam has a valley width exceeding 0.75 of its height and a slope greater than 45 degrees, it can be conclusively stated that the probability of horizontal arching induced by horizontal stresses is extremely low. Furthermore, the vertical arching phenomenon in the clay core becomes more pronounced when the core's width is less than 0.25 of its height, particularly under conditions where compaction levels do not achieve optimal moisture content. The occurrence of vertical arching is further mitigated in cores with a width-to-height ratio between 0.5 and 1, especially when the clay core is well-compacted within the optimal moisture content range (Fell *et al.*, 2015). In the case of the Balaroud reservoir dam, the maximum width of the clay core at the section of maximum embankment, section no. 4, measures 46 m, while the height is 82 m. Consequently, the width-to-height ratio is calculated to be 0.56, which falls within the range of 0.5 to 1. Therefore, the likelihood of vertical arching occurring within the core, along with the risk of hydraulic fracturing under static conditions, is assessed to be very low. Despite the reduced risk of arching, the importance of monitoring arching behavior in earthfill dams cannot be overstated. To ensure structural integrity, an evaluation and analysis of the arching ratio attributed to vertical stresses in the maximum section of the embankment was conducted. This assessment aims to enhance the understanding of stress distribution and reinforce the stability of the dam structure over time.

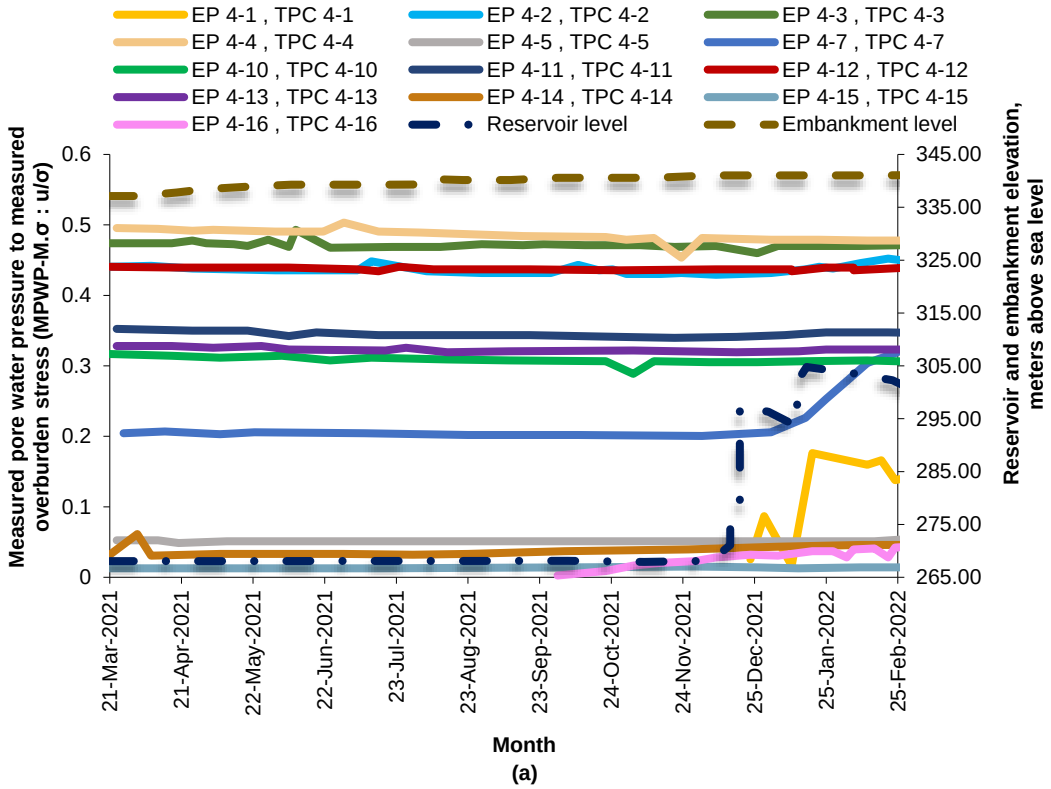

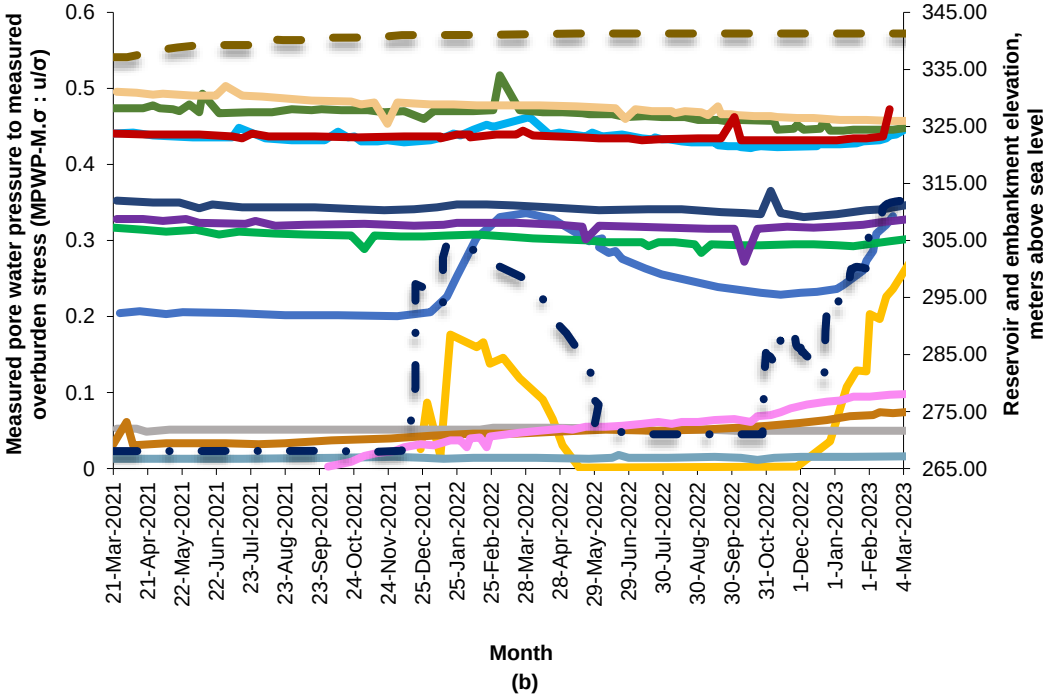

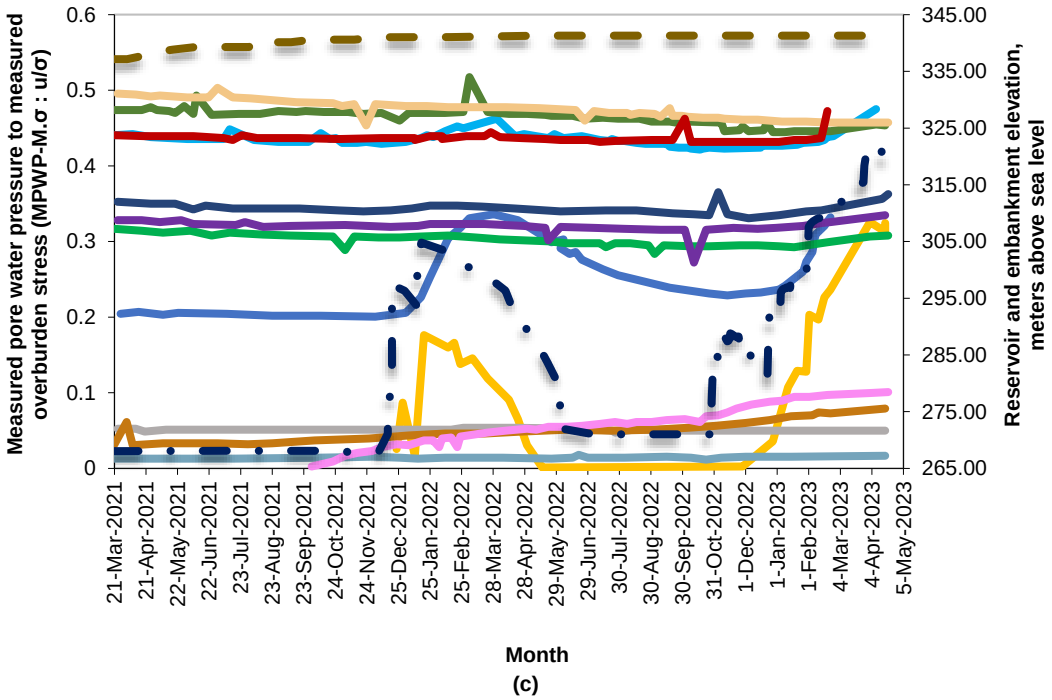

(c)

Fig. 14. Changes in the ratio of measured pore water pressure to measured overburden stress (MPWP-M.σ) during the (a) First, (b) Second, and (c) Third stages of impoundment.
Note: E.P. stands for "embankment piezometer" and T.P.C. stands for "total pressure cell". The numbers indicate their installation positions in the dam structure (refer to Fig. 7c).

3.4.1 First stage impoundment

The first stage of impoundment occurs at an elevation of 305 meters above sea level (m.a.s.l). Changes in the arching ratio (MTOS) during this process are depicted in Fig. 15a. It is clear from the figure that the MTOS values showed a slight decline over time across all total pressure cell (TPC) measurements. From May to December 2021,
the construction of the dam embankment resulted in a gradual increase in the height of the embankment, referred to as h. During this period, the reservoir remained empty, and no significant development of pore water pressure was detected within the dam structure. Consequently, due to minimal fluctuations in the overburden stress recorded by the TPC cells, a corresponding decrease in MTOS was noted. This situation continued until the completion of the embankment, at which point the height of the structure stabilized. Following this stabilization, the MTOS values remained constant until March 2022. The mean value of MTOS across all TPC cells was recorded at 0.494. This relatively low mean MTOS can be attributed to a localized arching phenomenon occurring at the locations where TPC cells were installed. This phenomenon led to the measured overburden stress being lower than expected. It has been noted that the installation of TPC cells occurred under constrained conditions, primarily due to the limitations of trench excavation and inadequate space for the necessary compaction of the embankment. Consequently, the localized arching may have been intensified during this installation process. At this stage of the impounding process, it is difficult to provide a definitive assessment regarding the extent or implications of this phenomenon. However, it is anticipated that as time progresses and the impounding process continues, along with the settlement of the dam body within acceptable limits, the localized arching effects will diminish. Therefore, it is expected that the measured values of overburden stress will approach their true values, thereby improving the reliability of the monitoring data collected from the TPC cells. This understanding will be vital for the ongoing assessment of the dam's structural integrity and performance.

3.4.2. Second stage impoundment

The second stage of impoundment occurs at an elevation of 310 meters above sea level (m.a.s.l). Changes in the arching ratio (MTOS) during this process are illustrated in Fig. 15b. Analysis of this figure indicates that the MTOS ratios in all TPC cells, except for TPC 4-4, show an increasing trend, occasionally stabilizing over time. Between March and November 2022, the gradual reduction and stabilization of the reservoir level, along with the completion of the dam embankment work, led to significant constancy in both the pore water pressure and the saturation zone. As a result, the measured overburden stress values remained approximately constant, leading to a fixed MTOS ratio during this period. From November 2022 to March 2023, as the reservoir level rose, a corresponding increase in pore water pressure and further development of the saturation zone was observed. This rise in pore water pressure, along with the increase in measured overburden stress, contributed to an increase in the MTOS ratio at most points within the dam body. The mean MTOS ratio across all TPC cells during this stage was recorded at 0.533, reflecting an 8 percent increase compared to the average values obtained during the first stage of the impounding process. This observed increase in the mean MTOS reinforces the conclusion that local arching phenomena had persisted and were influencing the stress measurements within the dam. It is anticipated that, as time progresses and the impounding process nears completion, along with the settlement of the dam body within allowable limits, the localized arching effects will diminish. Consequently, the measured values of overburden stress are expected to converge toward their actual values.

3.4.3. Third stage impoundment

The third stage of impoundment occurs at an elevation of 320 meters above sea level (m.a.s.l). Changes in the arching ratio (MTOS) during this process are illustrated in Fig. 15c. Analysis of this figure indicates that the MTOS ratios in all TPC cells, except for TPC 4-4, continue to exhibit an increasing trend, with certain periods characterized by stabilization. As the reservoir level rose further starting in March 2023, there was a corresponding increase in pore water pressure along with the development of the saturation zone, resulting in an increase in measured overburden stress. This combination of factors led to an upward trend in the MTOS ratio at most points within the dam's structure. The average MTOS ratio across all TPC cells during this stage was recorded at 0.586, representing an 18 percent increase compared to the average values from the first stage of the impounding process, and a 10 percent increase compared to those from the second stage.

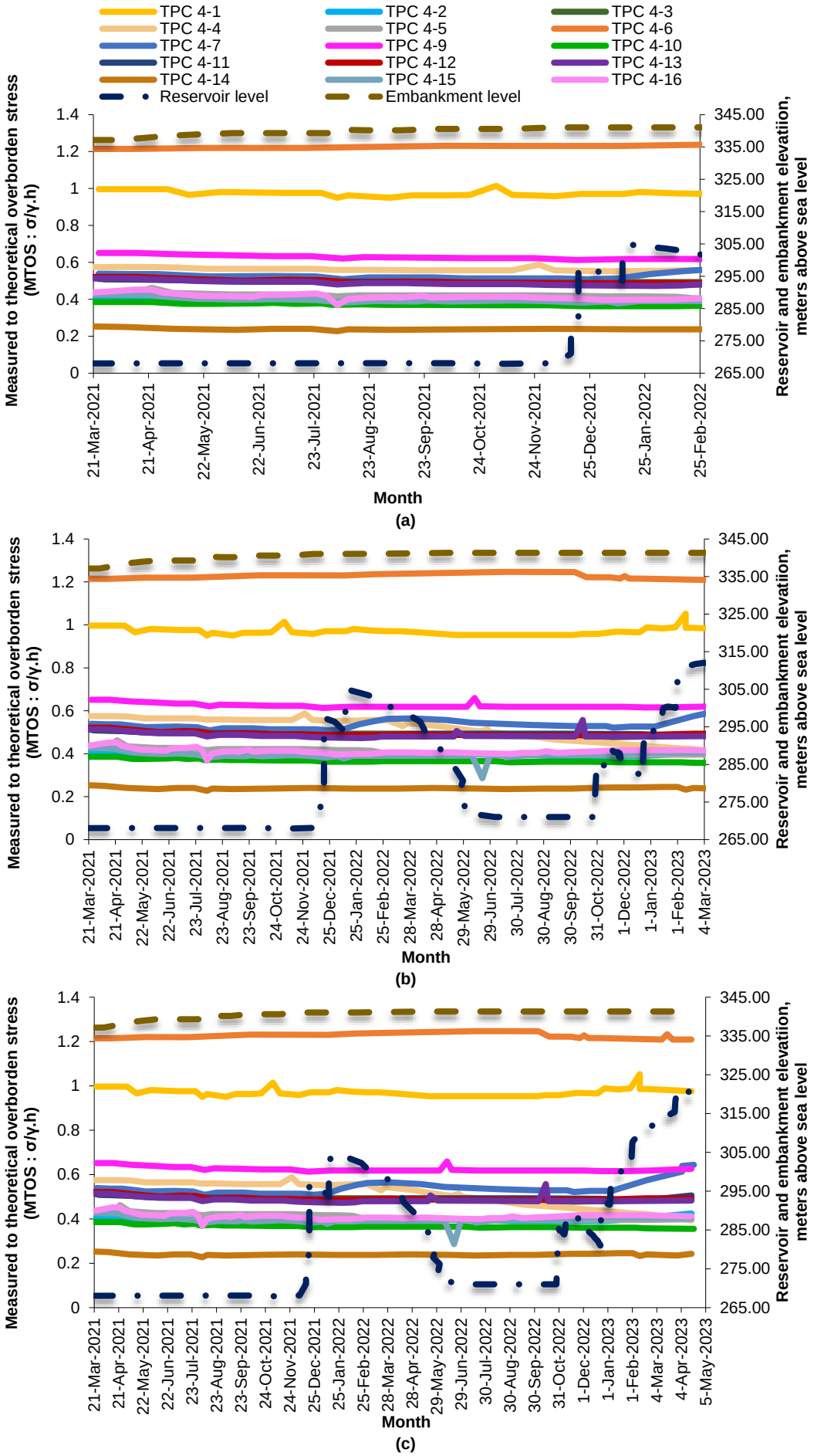

Fig. 15. Variations in the arching ratio: measured to theoretical overburden stress (MTOS) during (a) The first, (b) the second, and (c) the third stages of impoundment.

Note: T.P.C. stands for "total pressure cell". The numbers indicate their installation positions in the dam structure (refer to Fig. 7c).

This significant rise in the mean MTOS values reinforces the conclusion that localized arching phenomena remain active and are influencing stress distribution within the dam. Looking ahead, it is anticipated that as time progresses and the impounding process nears its conclusion, along with the settlement of the dam body within acceptable limits, the effects of local arching will diminish. Consequently, the measured overburden stress values are expected to approach their actual values, leading to an increase in the MTOS ratio. Continuous monitoring and assessment are imperative for evaluating the structural integrity of the dam and ensuring its long-term stability as it responds to evolving conditions. This knowledge will be crucial for guiding future operational decisions and maintenance strategies regarding the dam's performance and safety.

To thoroughly assess the impact of the MTOS ratio on dam stability, calculating the 1/PWPR is essential (Fell *et al.*, 2015; USBR, 2014). It was found that the most critical point related to sensors EP 4-14 and PC 4-14 recorded an average arching ratio of MTOS equal to 0.24 during the impounding process. At this location, the peak ratio of MPWP-M.σ reached 0.08, corresponding to an elevation of 321.75 meters above sea level in the third stage of impounding. Consequently, the maximum ratio of 1/PWPR is identified as 12.5, significantly exceeding the minimum acceptable threshold of 1.5. In light of these observations, the likelihood of liquefaction and internal erosion occurring within the Balaroud reservoir dam is considered very low.

4. Conclusions

The impoundment process, which began in May 2021, highlighted the vital role of the Balaroud dam in regional water resource management. The dam not only mitigates flood risks but also ensures a reliable and stable water supply downstream, thus supporting irrigation during dry periods and promoting ecological sustainability in the river environment. Instrumentation data indicated that initial pore water pressure variations were primarily due to embankment construction. After completion, these variations depended solely on reservoir level changes. Most SP and RP piezometers recorded pressures below the 800 kPa threshold. In the few piezometers exceeding this threshold, no anomalous increases in pore water pressure were observed alongside rises in overburden stress within TPC. The analysis of the pore water pressure ratio (PWPR) revealed that values remained within acceptable limits throughout the impounding process, with a maximum measured PWPR of 0.517—below the critical threshold of 0.521—indicating safe operation within design parameters. Initially, during embankment activities, PWPR values decreased due to increased effective stress from construction. In this study, the phenomenon of arching was also examined. During the initial stages of impoundment, low water levels in the reservoir, along with ongoing embankment activities, led to a slight decrease in the arching ratio (MTOS). This decrease was attributed to the absence of developed pore water pressure and an increase in embankment height. As the reservoir levels increased, the arching ratio rose, indicating an effective transfer of stress within the dam body. In conclusion, the findings indicate that embankment activities during the impoundment process had a minor impact on the data obtained from the instrumentation, thereby influencing the analysis of results and the monitoring of the stability of the Balaroud dam, albeit to a limited extent. Furthermore, the assessments confirm that the dam demonstrates favorable stability under current conditions, with a very low likelihood of phenomenon's such as hydraulic fracturing, liquefaction, or internal erosion. The data from this research can be utilized for simulating the reservoir water resources system and for calibrating numerical models. Additionally, future research can focus on monitoring this dam at the reservoir's normal level and at higher levels following the installation of spillway radial gates.

Nomenclature

u	Pore water pressure
σ	Overburden stress
PWPR	Pore water pressure ratio
MPWP-T.σ	Measured pore water pressure to theoretical overburden stress
MPWP-M.σ	Measured pore water pressure to measured overburden stress
MTOS	Arching ratio: measured to theoretical overburden stress
SP	Standpipe piezometer
RP	Rock piezometer
EP	Embankment piezometer
TPC	Total pressure cell
h	Embankment height

Conflict of Interest

The authors have no conflict of interest.

Data Availability Statement

The datasets used in the current study are available on request.

Acknowledgment

The authors would like to thank the Khuzestan Water & Power Authority (KWPA), Khuzestan, Iran, for providing the data, as well as Jundi-Shapur University of Technology, Dezful, Iran, for facilitating and supporting this research.

Author Contribution

Soroush Esmaeili-Zadeh: Data collection, writing—original draft of the manuscript.
Babak Lashkar-Ara: Review and editing of the manuscript, supervision, and corresponding author.

References

Anderson, L.R. (ed.) (1993). *Seepage control in dam rehabilitation, Proceedings of the Specialty Conference Geotechnical Practice in Dam Rehabilitation*. Raleigh, North Carolina, 25-28 April. New York City, United States: ASCE.

Beiranvand, B. and Komasi, M. (2019) 'Monitoring and numerical analysis of pore water pressure changes Eyvashan dam during the first dewatering period', *Journal of Applied Research in Water and Wastewater,* 6(1), pp. 1-7. doi: https://doi.org/10.22126/arww.2019.1017

Cavounidis, S. and Höeg, K. (1977) 'Consolidation during construction of earth dams', *Journal of the Geotechnical Engineering Division,* 103(10), pp. 1055-1067. doi: https://doi.org/10.1061/AJGEB6.0000496

Chong, K. L. *et al.* (2021) 'Review on dam and reservoir optimal operation for irrigation and hydropower energy generation utilizing meta-heuristic algorithms', *IEEE Access,* 9, pp. 19488-19505. doi: https://doi.org/10.1109/ACCESS.2021.3054424

Clements, R. P. (1984) 'Post-construction deformation of rockfill dams', *Journal of geotechnical engineering,* 110(7), pp. 821-840. doi: https://doi.org/10.1061/(ASCE)0733-9410(1984)110:7(82

Duncan, J. M. (1996) 'State of the art: limit equilibrium and finite-element analysis of slopes', *Journal of Geotechnical engineering,* 122(7), pp. 577-596. doi: https://doi.org/10.1061/(ASCE)0733-9410(1996)122:7(57

Eslami, A., Ghorbani, A. & Shahraini, S. V. (2020) 'Health monitoring and dynamic analysis of an earth-fill dam at the stage of first impounding: Case study—Siahoo dam of Iran', *Journal of Civil Structural Health Monitoring,* 10, pp. 425-442. doi: https://doi.org/10.1007/s13349-020-00393-5

Fatahi, M. and Lashkar-Ara, B. (2017) 'Estimating scour below inverted siphon structures using stochastic and soft computing approaches', *Journal of AI and Data Mining,* 5(1), pp. 55-66. doi: https://doi.org/10.22044/jadm.2016.757

Fathi, E. and Golestani, M. (2018) 'Instrumentation performance results in earth dams and comparing with numerical analysis: A case study on Doosti earth dam in Iran', *Electronic Journal of Geotechnical Engineering,* 23, pp. 271-292. Available at: https://www.academia.edu/79192455/Instrumentation_Performance_Results_in_Earth_Dams_and_Comparing_with_Numerical_Analysis_A_Case_Study_on_Doosti_Earth_Dam_in_Iran?sm=b (Accessed date: 10 December 2024).

Fetzer, C.A., Swiger, W.F. and Kramer, R.W. (1988) 'Earthfill Dam Construction and Foundation Treatment', In Jansen, R.B. (eds) *Advanced Dam Engineering for Design, Construction, and Rehabilitation*. Boston: Springer, pp. 321-353.

ICOLD (2023a) *Role Of Dams.* Available at: https://www.icold-cigb.org/GB/dams/role_of_dams (Accessed date: 11 December 2024).

ICOLD (2023b) *Number Of Dams By Country Members.* Available at: https://www.icold-

cigb.org/article/GB/world_register/general_synthesis/number-of-dams-by-country-members (Accessed date: 11 December 2024).

ICOLD (2023c) *Definition Of A Large Dam.* Available at: https://www.icold-cigb.org/GB/dams/definition_of_a_large_dam (Accessed date: 11 December 2024).

Komasi, M. and Beiranvand, B. (2019) 'Evaluation of pore water pressure foundation and core of Sivand dam after the first dewatering period in comparison with the actual instrument results', *Iranian Dam and Hydroelectric Powerplant,* 6(21), pp. 63-77. Available at: http://journal.hydropower.org.ir/article-1-304-en.html (Accessed date: 12 December 2024).

Lambe, T. W. (1973) 'Predictions in soil engineering', *Géotechnique,* 23(2), pp. 151-202. doi: https://doi.org/10.1680/geot.1973.23.2.151

Lashkar-Ara, b. & Kiani, f. (2025) 'Evaluating Optimal Relationships for Estimating Suspended Sediment Discharge in the Balaroud River', *Journal of Irrigation Sciences and Engineering,* 48(4), pp. 81-92. doi: https://doi.org/10.22055/JISE.2025.48205.2139

Lashkarara, B., Ghotbi, S. and Armaghani, A. (2012) 'Managing local scour downstream of cross-river structures case study: balaroud inverted siphon', *World Applied Sciences Journal,* 20(4), pp. 570-576. doi: https://doi.org/10.5829/idosi.wasj.2012.20.04.2706

Luo, D. *et al.* (2015) 'Effect of the impounding process on the overall stability of a high arch dam: a case study of the Xiluodu dam, China', *Arabian Journal of Geosciences,* 8, pp. 9023-9041. doi: https://doi.org/10.1007/s12517-015-1868-6

Marengo, H. (2006) 'Case study: dam safety during construction, lessons of the overtopping diversion works at Aguamilpa dam', *Journal of hydraulic engineering,* 132(11), pp. 1121-1127. doi: https://doi.org/10.1061/(ASCE)0733-9429(2006)132:11(1121)

Nezami, S. R. and Feizi, A. (2018) 'Achieving groundwater resource sustainability at watershed scale by conjunctive use of groundwater and surface resources', *Journal of Applied Sciences and Environmental Management,* 22(8), pp. 1263-1268. doi: https://doi.org/10.4314/jasem.v22i8.19

Oral, Y. Z. (2010) *Deformation behavior of a clay cored rockfill dam in Turkey.* Master's thesis. Middle East Technical University. Available at: http://etd.lib.metu.edu.tr/upload/12612886/index.pdf (Accessed date: 15 December 2024).

Pagano, L., Desideri, A. and Vinale, F. (1998) 'Interpreting settlement profiles of earth dams', *Journal of geotechnical and geoenvironmental engineering,* 124(10), pp. 923-932. doi: https://doi.org/10.1061/(ASCE)1090-0241(1998)124:10(923)

Fell, R. *et al.* (2015). *Geotechnical Engineering of Dams*. 2th edn. Netherlands: CRC Press.

Radzicki, K. and Stoliński, M. (2024) 'Seepage monitoring and leaks detection along an earth dam with a multi-sensor thermal-active system', *Bulletin of Engineering Geology and the Environment,* 83(9), p. 362. doi: https://doi.org/10.1007/s10064-024-03826-3

Saab, S. M. *et al.* (2022) 'Review on generating optimal operation for dam and reservoir water system: simulation models and optimization algorithms', *Applied Water Science,* 12(4), p. 73. doi: https://doi.org/10.1007/s13201-022-01593-8

Salimi, N. *et al.* (2021) 'Management and planning of water resources allocation at the scenario analysis using system dynamics model: A case study on Yamchi dam basin, Iran', *Journal of applied research in water and wastewater,* 8(1), pp. 14-20. doi: https://doi.org/10.22126/arww.2021.6453.1211

Sharma, H. D. (1991) *Embankment Dams*. New Delhi: Oxford & IBH Publishing Company.

Siriwardane, H.J. and Zaman, M.M. (eds.) (1994). *Proceedings of the Eighth International Conference on Computer Methods and Advances in Geomechanics*. Morgantown, West Virginia, USA, 22-28 May 1994. Netherlands: A.A. Balkema. Volume 3.

USBR (2014) *DS-13(8)-4.1: Design Standards Embankment Dams, Seepage*. United States: U.S. Department of Interior Bureau of Reclamation.

Vasconcelos, R. P. *et al.* (2015) 'Global patterns and predictors of fish species richness in estuaries', *Journal of Animal Ecology,* 84(5), pp. 1331-1341. doi: https://doi.org/10.1111/1365-2656.12372

Yaseen, Z. M. *et al.* (2019) 'A hybrid bat–swarm algorithm for optimizing dam and reservoir operation', *Neural Computing and Applications,* 31, pp. 8807-8821. doi: https://doi.org/10.1007/s00521-018-3952-9

Yun, S.-K. *et al.* (2022) 'Behavior of porewater pressures in an earth dam by principal component analysis', *Water,* 14(4), pp. 672. doi: https://doi.org/10.3390/w14040672